Journal of Orthopaedic Translation 49 (2024) 325–338

Contents lists available at ScienceDirect

Journal of Orthopaedic Translation

journal homepage: www.journals.elsevier.com/journal-of-orthopaedic-translation

Original Article

Sensory nerve EP4 facilitates heterotopic ossification by regulating angiogenesis-coupled bone formation

Rongmin Lin [a,b,1], Hancheng Lin [a,b,1], Chencheng Zhu [a,b], Jieming Zeng [e], Jiahui Hou [a,b], Ting Xu [c], Yihui Tan [d], Xuyou Zhou [a,b], Yuan Ma [a,b], Mankai Yang [a,b], Kuanhai Wei [a,b], Bin Yu [a,b,**], Hangtian Wu [a,b,***], Zhuang Cui [a,b,*]

[a] Department of Orthopaedics and Traumatology, Nanfang Hospital, Southern Medical University, Guangzhou, Guangdong, 510515, China
[b] Key laboratory of bone and cartilage regeneration medicine, Southern Medical University, Guangzhou, Guangdong, 510515, China
[c] Department of Sleep Medicine Center, Nanfang Hospital, Southern Medical University, Guangzhou, Guangdong, 510515, China
[d] The Affiliated TCM Hospital of Guangzhou Medical University, Guangzhou, Guangdong, 510130, China
[e] Guangzhou Hospital of Integrated Traditional and Western Medicine, Guangzhou, Guangdong, 510515, China

ARTICLE INFO

Keywords:
Angiogenesis
Efnb2
EP4
Heterotopic ossification
Sensory nerve

ABSTRACT

Objective: Heterotopic ossification (HO) refers to the abnormal development of bone in soft tissue rather than within bone itself. Previous research has shown that sensory nerve prostaglandin E2 receptor 4 (EP4) signaling not only governs pain perception but also influences bone formation. However, the relationship between sensory nerve EP4 and the pathogenesis of HO in the Achilles tendon remains unclear. This study aims to investigate this relationship and the underlying mechanisms.

Methods: We generated sensory nerve EP4-specific knockout mice, with the genotype of Avil-CreEP4$^{fl/fl}$, was propagated. Transcriptome sequencing and bioinformatics analysis techniques were used to identify the potential molecular pathways involving with sensory nerve EP4. Additionally, a neurectomy mouse model was created by transecting the sciatic nerve transection, to examine the effects and mechanisms of peripheral innervation on HO in vivo. Micro-CT, immunofluorescence (IF), Hematoxylin and Eosin (H&E) Staining, Safranin O-Fast Green staining and western blotting were used to analyze changes in cellular and tissue components.

Results: We here observed an increase in sensory nerve EP4 and H-type vessels during the pathogenesis of HO in both human subjects and mice. Proximal neurectomy through sciatic nerve transection or the targeted knockout of EP4 in sensory nerves hindered angiogenesis-dependent bone formation and the development of HO at the traumatic site of the Achilles tendon. Furthermore, we identified the Efnb2 (Ephrin-B2)/Dll4 (Delta-like ligand 4) axis as a potential downstream element influenced by sensory nerve EP4 in the regulation of HO. Notably, administration of an EP4 inhibitor demonstrated the ability to alleviate HO. Based on these findings, sensory nerve EP4 emerges as an innovative and promising approach for managing HO.

Conclusion: Our findings demonstrate that the sensory nerve EP4 promotes ectopic bone formation by modulating angiogenesis-associated osteogenesis during HO.

The translational potential of this article: Our results provide a mechanistic rationale for targeting sensory nerve EP4 as a promising candidate for HO therapy.

1. Introduction

Heterotopic ossification (HO) refers to the formation of bone in tissues where it does not normally occur, such as in soft tissue [1]. HO can be either congenital or acquired, with most patients developing acquired HO rather than being born with it (congenital) [2]. Acquired

* Corresponding author. Department of Orthopaedics and Traumatology, Nanfang Hospital, Southern Medical University, Guangzhou, Guangdong, 510515, China.
** Corresponding author. Department of Orthopaedics and Traumatology, Nanfang Hospital, Southern Medical University, Guangzhou, Guangdong, 510515, China.
*** Corresponding author. Department of Orthopaedics and Traumatology, Nanfang Hospital, Southern Medical University, Guangzhou, Guangdong, 510515, China.
E-mail addresses: yubinol@163.com (B. Yu), wuhangtian@smu.edu.cn (H. Wu), cuizhuang@smu.edu.cn (Z. Cui).
[1] These authors contributed equally

https://doi.org/10.1016/j.jot.2024.09.005
Received 3 June 2024; Received in revised form 22 August 2024; Accepted 24 September 2024

HO is a common and high-incidence clinical complication following trauma, such as tendon injuries, fractures, central nervous system injuries, total hip replacements, and severe burns [3]. This condition can lead to significant clinical issues, including pain, inflammation, contracture development, restricted joint mobility, and even loss of limb function, significantly affecting daily activities [4]. Current treatment options for HO, such as non-steroidal anti-inflammatory drugs, radiotherapy, and/or surgical excision, are limited and often result in high recurrence rates. Recurrence is observed in up to 58 % of patients clinically symptoms and in nearly 100 % of patients on imaging. Additionally, these treatments can lead to other complications [5]. This high recurrence rate is due to an incomplete understanding of the underlying causes of HO. Therefore, further exploration of the pathogenesis of HO and the development of new therapeutic approaches are of significant clinical importance.

Post-traumatic pain is often the initial clinical presentation of HO, followed by inflammatory reactions, soft tissue adhesions, and heterotopic ossification [6,7]. In addition, injuries to the central nervous system (CNS) often contribute to the development of HO [3]. These clinical observations suggest that sensory nerve innervation may play a role in trauma-induced HO. Recent research has shown that after soft tissue injury, sensory nerves stimulated by nerve growth factor (NGF) migrate toward the site of HO [8]. However, the specific mechanisms through which sensory nerves contribute to ectopic ossification remain unclear. Sensory nerves are integral for collecting signals from both internal and external environments, enabling individuals to respond to their surroundings [9]. Notably, it has been reported that sensory nerve prostaglandin E2 receptor 4 (EP4) can detect a bone-forming "signal" called prostaglandin E2 (PGE2), which plays a role in regulating bone homeostasis [10]. Furthermore, the deletion of the EP4 gene in sensory nerves has been associated with reduced bone mass [10]. Additionally, sensory nerve EP4 has been shown to regulate the osteogenic commitment of mesenchymal stem cells (MSCs) by modulating sympathetic tones [11]. Therefore, sensory nerve EP4 may play a crucial role in the pathogenesis of ectopic ossification. Moreover, bone formation is often accompanied by angiogenesis, a process coordinated by a specific subtype of vessels known as H-type or $CD31^{hi}Emcn^{hi}$ vessels [12]. Our previous research has shown that H-type vessels establish a beneficial feedback loop with MSCs during the onset of osteoarthritis [13]. However, the role of sensory nerves in regulating angiogenesis-dependent bone formation in the pathogenesis of HO has not been fully understood.

In this study, we observed an increase in sensory nerve EP4 and H-type vessels during the development of HO in both human subjects and mouse models. In addition, targeted disruption of EP4 in sensory nerves

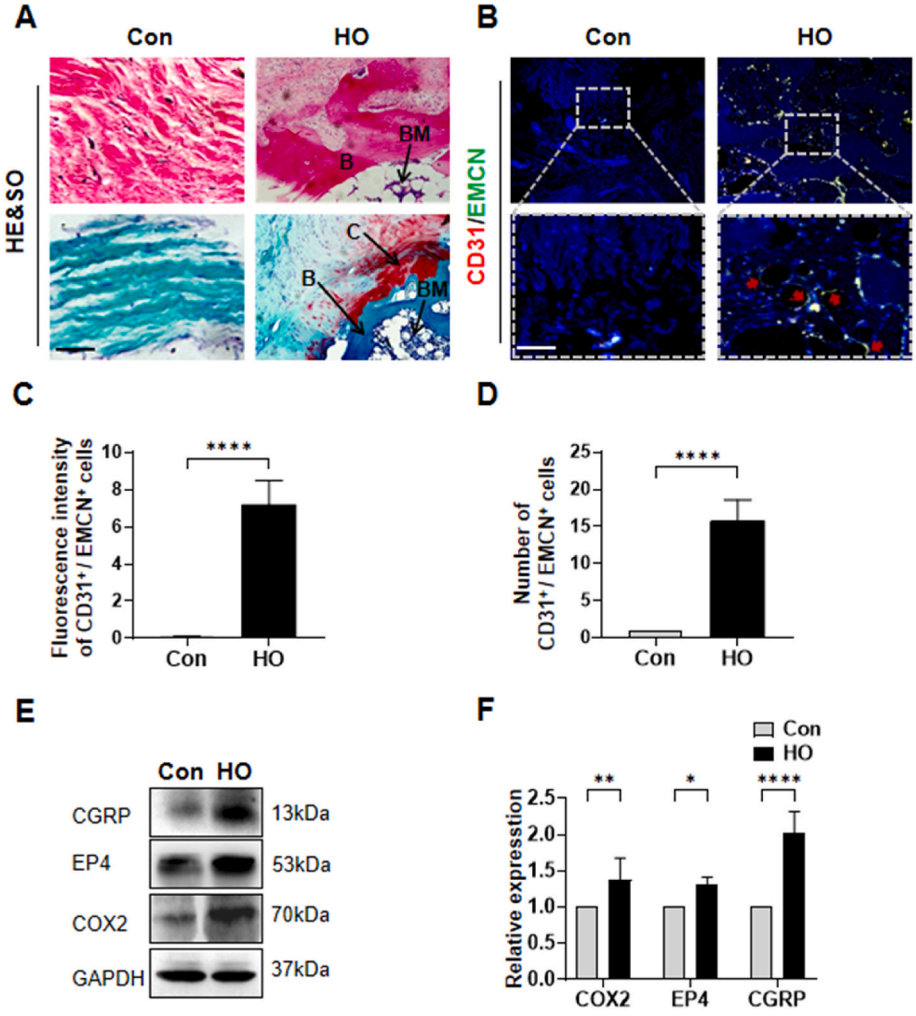

Fig. 1. Sensory nerve EP4 is upregulated in human HO specimens (A) H&E staining and Safranin O and Fast Green (SOFG) staining of control (muscle tissue) and HO tissue (B: bone; BM: bone marrow; C: cartilage). Proteoglycan (red) and heterotopic bone (green). Scale bar, left 25 μm), right 100 μm (B) Immunostaining of H-type vessels (endomucin: green; CD31: red; merge: yellow) in human specimen of the control and HO tissue (red arrows: H-type vessels). Scale bar, bottom 25 μm; top 100 μm (C, D) Quantification of fluorescence intensity and number of $CD31^{+}/EMCN^{+}$ cells related to control in human specimen of the control and HO tissue. n = 5 (E) Western blot examination of expression of CGRP, EP4 and COX2 in control or HO tissue of human (F) Quantification of protein level of CGRP, EP4 and COX2 normalized to GAPDH. n = 5 (*P < 0.05 **P < 0.01 ****P < 0.0001 compared to the control group or as denoted by bars).

inhibited angiogenesis-dependent bone formation and the pathogenesis of HO. Furthermore, we identified the Efnb2 (Ephrin-B2)/Dll4 (Delta-like 4) axis as a downstream component of sensory nerve EP4 that regulates HO. Based on these findings, sensory nerve EP4 emerges as an innovative and promising strategy for addressing HO.

2. Results

2.1. Sensory nerve EP4 is elevated in both human HO patients and in a mouse HO model

We initially analyzed surgical specimens from patients with acquired HO, which had been radiographically identified following internal fixation for elbow fractures. Hematoxylin and eosin (H&E) and Safranin O-Fast Green staining results confirmed the occurrence of typical ectopic bone formation (Fig. 1A). Consistent with previous reports that bone formation often coincides with angiogenesis [14], our observations revealed the presence of H-type vessels, identified through dual immunostaining for endomucin (EMCN) and CD31 (Fig. 1B–D), Additionally, the osteogenic gene *OSX* (Osterix) was detected in HO tissues (Figs. S1A and B). Post-traumatic pain precedes the pathogenesis of HO, and previous studies have confirmed that sensory nerve EP4/PGE2 signaling not only regulates pain responses but also bone formation [10]. Given this, we proceeded to investigate alterations in sensory nerve levels within the HO tissue of human subjects. As regards calcitonin gene-related peptide (CGRP), it is a neuropeptide possessing multiple physiological functions and is prevalently expressed in sensory nerves throughout the body [15]. Prior studies have employed double immunostaining of CGRP and EP4 to detect the expression of EP4 in sensory nerve fibers [10,16]. Cycloxygenase 2 (Cox-2) is a essential enzyme for the generation of prostaglandin E2 (PGE2), which serves as the ligand of sensory nerve EP4 for sensing pain and governing bone formation [10,17]. Cox2-selective inhibitors are not merely the prevailing principal medications for treating musculoskeletal pain [18], but also correlated with a lower bone mineral density (BMD) in men [19]. Previous investigations have utilized the expression modification of Cox-2 to mirror PGE2 [10, 20]. Western blot analysis revealed a significant increase in levels of CGRP, EP4, and COX2 in the pathogenesis of human HO compared to the control group (Fig. 1E and F). We subsequently evaluated the sensory nerve EP4 expression in HO of a mouse model with tenotomy. Consistent with the aforementioned discoveries, the micro-CT scan revealed the presence of ectopic ossification within the Achilles tendon of mice post-tenotomy (Fig. 2A and B). Concurrently, we observed that H-type vessels increased alongside the formation of ectopic ossification, with the most notable changes occurring at 10 weeks post-Achilles tenotomy (Fig. 2C–E). Furthermore, the expression of sensory nerves was similar to that of H-type vessels, as indicated by double immunostaining of CGRP and EP4, which revealed the most significant colocalization at 10 weeks (Fig. 2F and G). In addition, the osteogenesis index *OSX* was also significantly increased after Achilles tendon HO modeling (Figs. S1C and D). These findings suggest a strong correlation between sensory nerve EP4 and angiogenesis-driven bone formation.

2.2. Proximal neurectomy prevents the onset of HO in mice

To further investigate the necessity of nerve invasion in HO, we induced HO under conditions of surgical denervation [8]. We transected the sciatic nerve on the same side where the Achilles tendon surgeries were performed to establish the impact of sensory nerve deletion on HO. Although there exist numerous researches delving into the impact of sciatic nerve transection upon HO [8,21], nevertheless, whether the sciatic nerve transection influences the angiogenesis-related bone formation has not been examined during the advent of HO. As anticipated, the expression of sensory nerve EP4 in the Achilles tendon of the denervated group showed a significant decrease compared to the sham group (Fig. 3A–C). Furthermore, we observed a marked reduction in H-type vessels and in the expression of OSX, as demonstrated by immunostaining (Fig. 3D–F, Figs. S1E and F). Consistently, H&E staining, Safranin O-Fast Green staining, and micro-CT analysis unveiled a significant decrease in ectopic bone formation following surgical denervation compared to the sham group (Fig. 3G–J). Collectively, these findings indicate that peripheral innervation may serve a crucial function in the pathogenesis of HO.

2.3. EP4 knockout in sensory nerves reduces HO in mice

Previous studies have demonstrated that sensory nerve EP4 is capable of regulating bone formation [10]. However, it remains unclear whether this regulation is crucial for HO development. To investigate this, we specifically deleted EP4 in sensory nerves ($EP4^{-/-}_{Avil}$) by the mating mice carrying the loxP-flanked EP4 allele ($EP4^{lox/lox}$) with Advillin-cre transgenic mice to validate the function of sensory nerves EP4 during HO. Littermate mice ($EP4^{lox/lox}$) were used as controls to avoid any genetic interference. The results of H&E staining, Safranin O-Fast Green staining, and micro-CT showed a significant reduction in HO following the knockout of sensory nerve EP4 compared to the control group (Fig. 4A–D). Additionally, immunostaining revealed a decrease in the abundance of H-type vessels and OSX after gene knockdown treatment (Fig. 4E–G, Figs. S2A and B). We also evaluated the expression of CGRP and EP4 in gene knockdown mice and found minimal EP4 expression or colocalization with CGRP (Figs. S2C–E). However, sensory nerve expression did not differ in the distal tibial adjacent to the trauma site between the control and HO groups (Figs. S2F and G). This indicates that knockout EP4 in sensory nerve does not lead to widespread denervation and that sensory nerve EP4 may potentially modulate the pathogenesis of HO by regulating angiogenesis-dependent bone formation.

2.4. Sensory nerve EP4 promotes HO probably through the function of Efnb2-mediated Dll4-related notch signaling

To explore the mechanisms by which sensory nerve EP4 affects HO, we performed RNA-sequencing on lesion tissues of the Achilles tendon collected at 10 weeks after surgical induction. We used sensory nerve-specific EP4 knockout mice ($EP4^{-/-}_{Avil}$) and compared them to $EP4^{wt}$ mice. The stability of the specimens was reflected in Violin plots, Pearson's correlation diagrams and transcripts per million distributions (Fig. 5A, Fig. S3A and B), showing excellent biological reproducibility [22]. After analyzing the differences between the two sample groups, we identified 637 genes exhibiting with significant variance, as shown in the presented bar chart, volcano plot and heatmap (Fig. 5B and C, Fig. S3C). Genes with up-regulated expression are highlighted in red, while those with down-regulated expression are highlighted in blue. To understand potential regulators, we conducted Gene Ontology (GO) enrichment analysis on the significantly differentially expressed genes. Bone formation often coincides with angiogenesis [23], and our previous research has shown that H-type vessels have a mutually beneficial relationship with MSCs during osteoarthritis initiation [13]. Therefore, we hypothesized that sensory nerve EP4 might influence HO pathogenesis by affecting angiogenesis-driven bone formation. We identified angiogenesis-related functions ($p < 0.05$) in the GO database, with "Angiogenesis" being the most significant and involving the largest number of differential genes (37 genes), as shown in Fig. 5D. Genes associated with "Angiogenesis" are displayed in the heatmap (Fig. 5E). The *Efnb2* gene caught our interest, as it had the highest correlation within the angiogenesis GO enrichment function, and it was also among the top 20 significant differential genes overall (Fig. 5F). Further analysis using protein–protein interaction (PPI) network software (Fig. 5G) revealed that the *Efnb2* gene had the strongest correlation with *Dll4* gene among all notable differentially expressed genes, with Efnb2 positively regulating Dll4. Notably, Dll4 is a key ligand in the traditional Notch-signaling pathway, suggesting that Efnb2 may trigger this

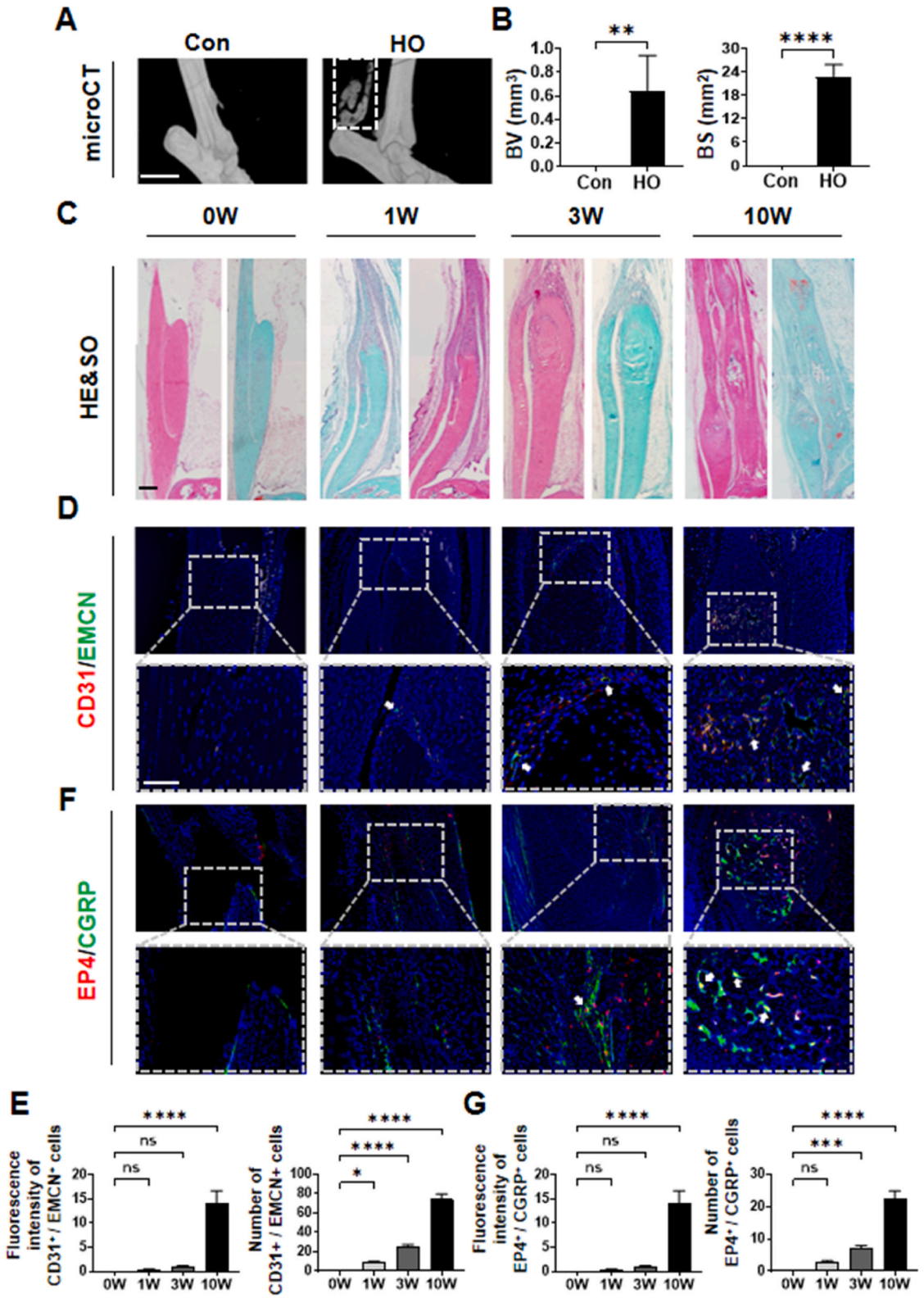

Fig. 2. Sensory nerve EP4 is elevated in trauma site of Achilles tendon in mice (A) Micro CT images of ectopic bone formation in Achilles tendon (sagittal view) after sham operation (control group) or at 10 weeks (HO group) after tenotomy (B) Quantitative analysis of bone volume (BV) and bone surface (BS). n = 5. Scale bar, 2 mm (C) H&E staining and Safranin O and Fast Green (SOFG) staining of mice Achilles tendon (sagittal view) at 0, 1, 3, 10 weeks after tenotomy. Proteoglycan (red) and heterotopic bone (green). Scale bar, 100 μm (D) Immunostaining of H-type vessels (endomucin: green; CD31: red; merge: yellow) in mice Achilles tendon (sagittal view) at 0, 1, 3, 10 weeks after tenotomy. Scale bar, bottom 50 μm; top 100 μm (E) Quantification of fluorescence intensity and number of $CD31^{+}/EMCN^{+}$ cells related to control in mice. 0W group was set as the control group. n = 5 (F) Immunostaining of sensory nerve EP4 (CGRP (representing sensory nerve): green; EP4: red; merge: yellow) in mice Achilles tendon (sagittal view) at 0, 1, 3, 10 weeks after tenotomy. Scale bar, bottom 50 μm; top 100 μm (G) Quantification of fluorescence intensity of and number of $EP4^{+}/CGRP^{+}$ cells in mice. 0W group was set as the control group. n = 5 (ns $p > 0.1$ *$P < 0.05$ ***$P < 0.001$ ****$P < 0.0001$ compared to the control group or as denoted by bars).

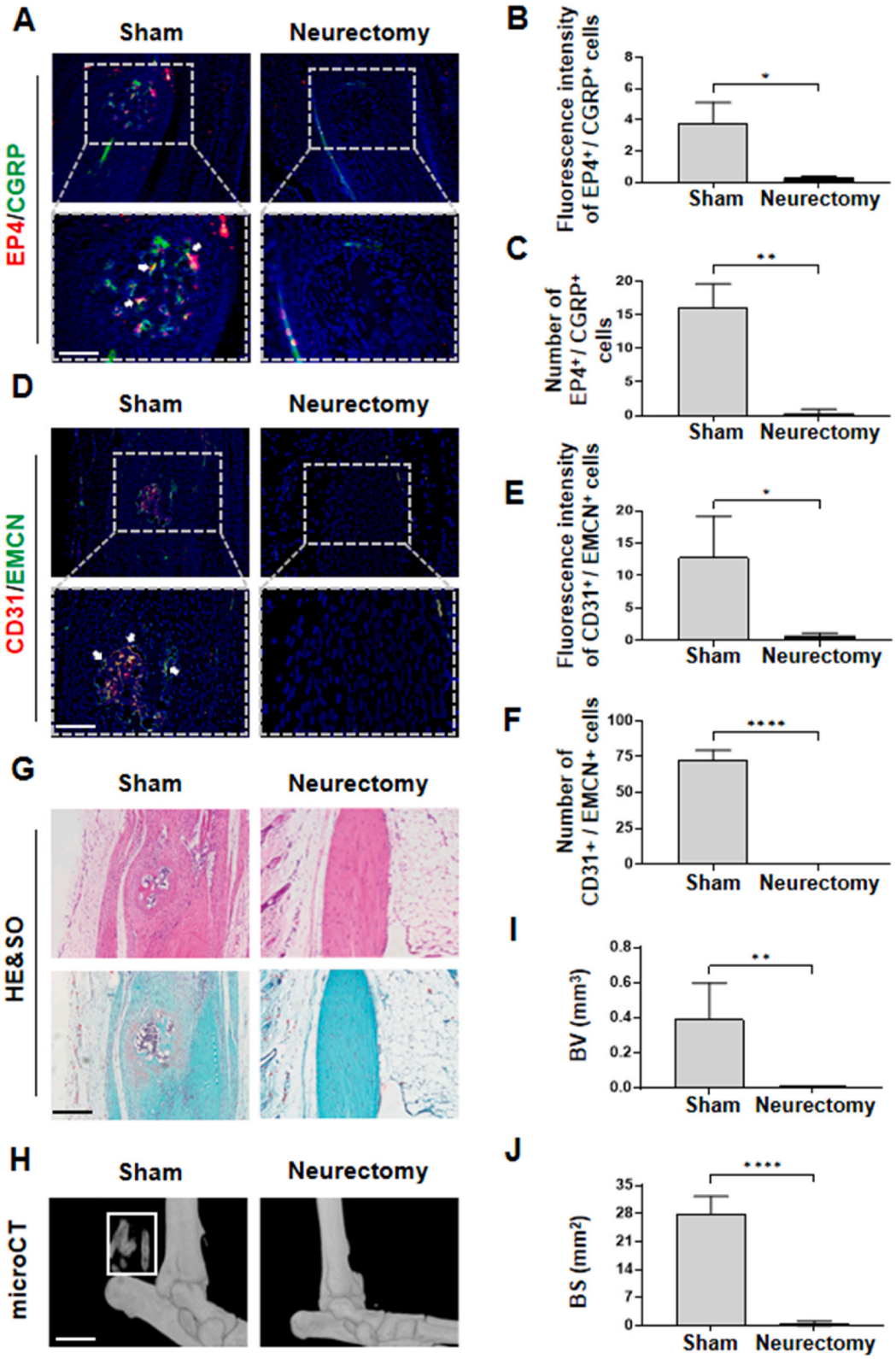

Fig. 3. Performing sciatic nerve transection in mice averts the initiation of HO (A) Immunostaining of sensory nerve EP4 (CGRP: green; EP4: red; merge: yellow) in mice Achilles tendon after 10 weeks of traumatic induced HO with or without proximal sciatic neurectomy. Scale bar, bottom 50 μm; top 100 μm (B, C) Quantification of fluorescence intensity and number of $EP4^{+}/CGRP^{+}$ cells, n = 5 (D) Immunostaining of H-type vessels (endomucin: green; CD31: red; merge: yellow) in mice Achilles tendon (sagittal view) after 10 weeks of traumatic induced HO with or without proximal sciatic neurectomy. Scale bar, bottom 50 μm; top 100 μm (E, F) Quantification of fluorescence intensity and $CD31^{+}/EMCN^{+}$ cells related to control. n = 5 (G) H&E staining and Safranin O and Fast Green (SOFG) staining of mice Achilles tendon (sagittal view) after 10 weeks of traumatic induced HO with or without proximal sciatic neurectomy. Proteoglycan (red) and heterotopic bone (green). Scale bar, 100 μm (H) Micro CT images of ectopic bone formation in Achilles tendon (sagittal view) after 10 weeks of traumatic induced HO with or without proximal sciatic neurectomy (I, J) Quantitative analysis of bone volume (BV) and bone surface (BS). n = 5. Scale bar, 2 mm (*P < 0.05 **P < 0.01 ****P < 0.0001 compared to the sham group or as denoted by bars).

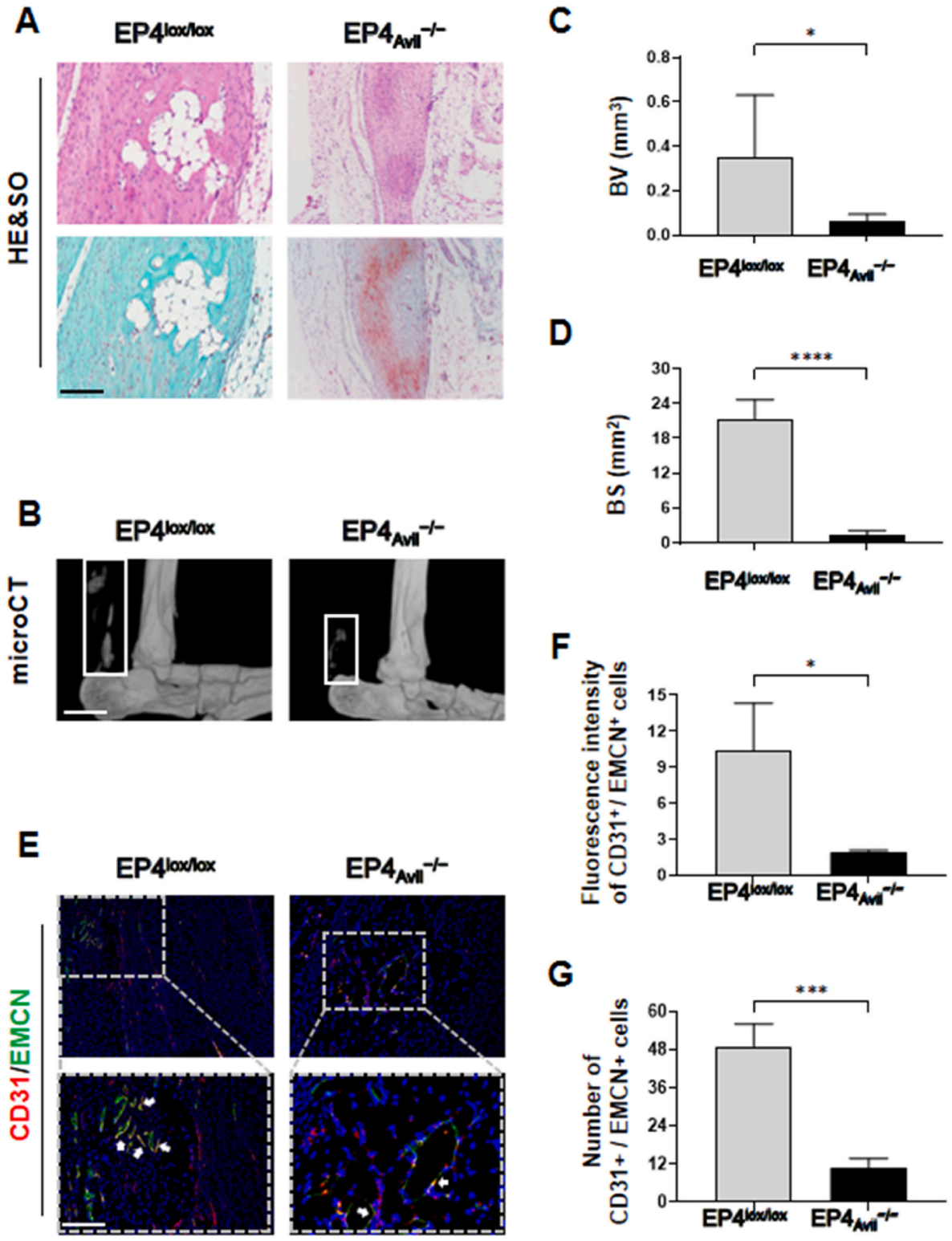

Fig. 4. Disabling EP4 in sensory nerves diminishes heterotopic ossification in mice (A) H&E staining and Safranin O and Fast Green (SOFG) staining of transgenic mice Achilles tendon (sagittal view) after 10 weeks of traumatic induced HO. Proteoglycan (red) and heterotopic bone (green). $EP4^{lox/lox}$ mice were treated as a control group. Scale bar, 100 μm (B) Micro CT images of ectopic bone formation in $EP4^{lox/lox}$ or $EP4_{Avil}^{-/-}$ mice Achilles tendon (sagittal view) after 10 weeks of traumatic induced HO (C, D) Quantitative analysis of bone volume (BV) and bone surface (BS). n = 5. Scale bar, 2 mm (E) Immunostaining of H-type vessels (endomucin: green; CD31: red; merge: yellow) in $EP4^{lox/lox}$ or $EP4_{Avil}^{-/-}$ mice Achilles tendon (sagittal view) after 10 weeks of traumatic induced HO. Scale bar, bottom 50 μm; top 100 μm (F, G) Quantification of fluorescence intensity and $CD31^{+}/EMCN^{+}$ cells. n = 5 (*P < 0.05 ***P < 0.001 ****P < 0.0001 compared to the control group or as denoted by bars).

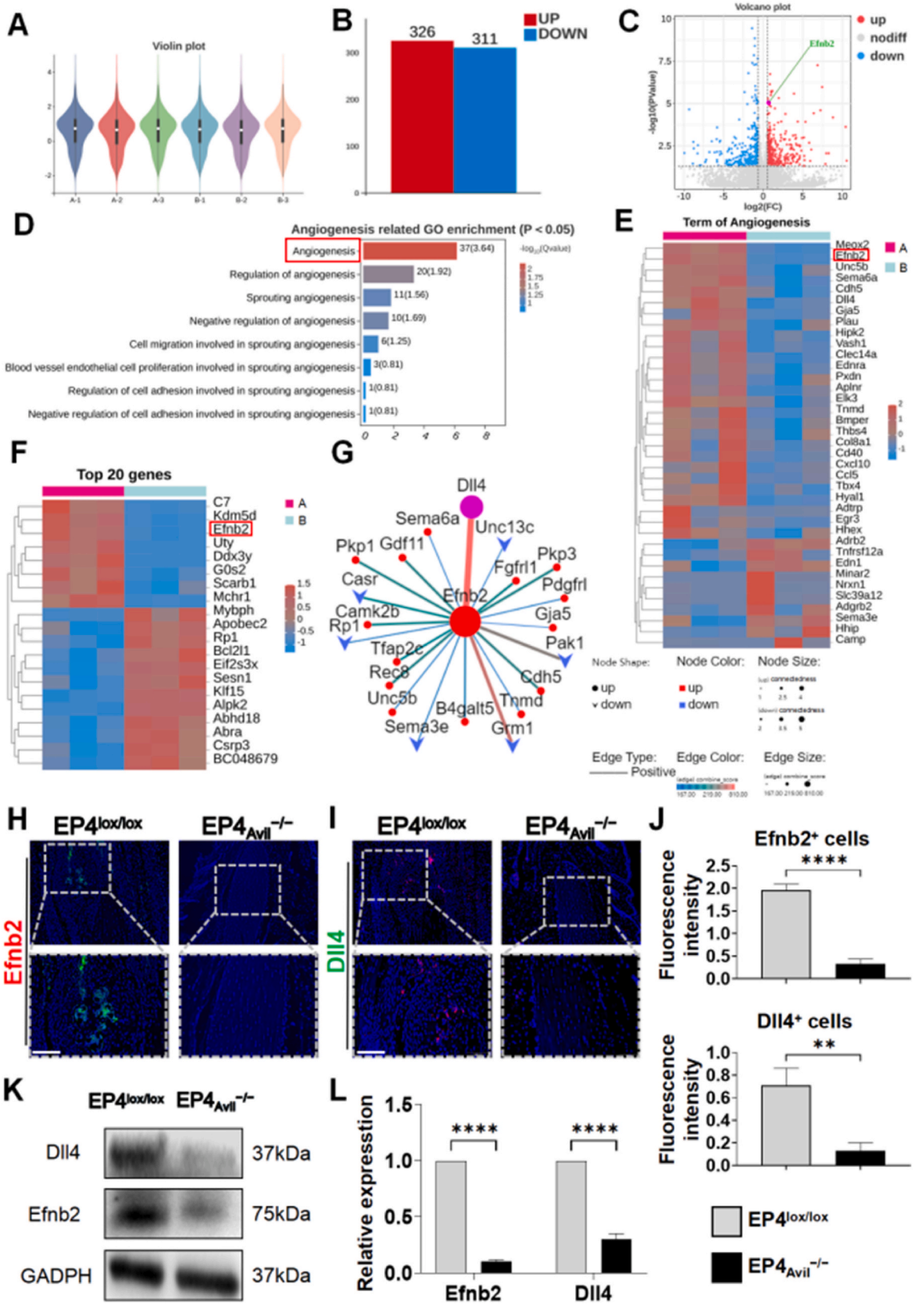

(caption on next page)

Fig. 5. The promotion of HO by sensory nerves EP4 likely occurs via Efnb2/Dll4 axis (A) Violin plot representing stability among specimens of each group. The samples harvested from $EP4^{lox/lox}$ were group A (A1-A3), from $EP4^{-/-}_{Avil}$ were Group B (B1-B3) (B) Bar chart of differential gene expression between samples. Difference multiple was set from −1.5 to 1.5. $P < 0.05$ (C) Volcano plot for transcriptome analysis of differentially expressed genes. Efnb2 gene was highlighted. Difference multiple was set from −1.5 to 1.5. $P < 0.05$ (D) Angiogenesis-related functions from the GO enrichment database. $P < 0.05$ (E) Heat map of genes located in function of Angiogenesis from GO enrichment (F) Heat map of top 20 genes with significantly differential gene expression. Difference multiple was set from −1.5 to 1.5. $P < 0.05$ (G) Target gene PPI network of Efnb2 gene. Thicker line represented stronger gene correlation. Ellipse represented positive regulation, the vee represented negative regulation (H) Immunostaining of Efnb2 (green) in $EP4^{lox/lox}$ or $EP4^{-/-}_{Avil}$ mice Achilles tendon (sagittal view) after 10 weeks of traumatic induced HO. Scale bar, bottom 50 μm; top 100 μm (I) Immunostaining of Dll4 (red) in $EP4^{lox/lox}$ or $EP4^{-/-}_{Avil}$ mice Achilles tendon (sagittal view) after 10 weeks of traumatic induced HO. Scale bar, bottom 50 μm; top 100 μm (J) Quantification of fluorescence intensity of $Efnb2^{+}$ cells and $Dll4^{+}$ cells. n = 5 (K) Western blot examination of expression of Efnb2 and DLL4 in $EP4^{lox/lox}$ or $EP4^{-/-}_{Avil}$ mice Achilles tendon after traumatic induced HO (L) Quantification of protein level of Efnb2 and Dll4 normalized to GAPDH (**$P < 0.01$ ****$P < 0.0001$ compared to the control group or as denoted by bars).

pathway, which plays a central role in H-type vessel formation [14]. We examined the expression of Efnb2 and Dll4 through immunofluorescence and western blotting in the trauma site of the Achilles tendon (Fig. 5H–L). Our findings showed a significant increase in the expression of these two markers in $EP4^{lox/lox}$ mice compared to $EP4^{-/-}_{Avil}$mice.

To further confirm the role of the Efnb2/Dll4 axis in angiogenesis mediated by sensory nerve EP4, we silenced EP4 in SH-SY5Y cells using small interfering RNA and selected siEP4#1 with the best interference effect as the siRNA for silencing EP4 in subsequent experiments (Fig. 6A and B). Upon stimulation with PGE2, EP4 knockdown in SH-SY5Y cells led to decreased Efnb2 and DII4 expression (Fig. 6C and D). The supernatant from SH-SY5Y cells treated under various conditions was then used to co-culture bone marrow endothelial cells (BMECs) for further experiments. The tube formation assay conducted using Matrigel revealed that the supernatant from SH-SY5Y cells upon stimulation by PGE2 facilitates vessel formation, while this function was hindered when inhibiting its EP4, Efnb2 or Dll4 signaling by means of the relevant interfering RNA (Fig. 6E–G). Meanwhile, we discovered that the deletion of EP4 in the SH-SY5Y cells inhibits its role in vessel formation; however, Efnb2 or Dll4 stimulation has the ability to reverse this phenomenon (Fig. 6E–G). A scratch wound healing assay (Fig. 6H–J) yielded similar results, indicating that the removal of *EP4*, *Efnb2*, or *Dll4* from neural cells attenuated the motility of BMECs following supernatant treatment. Nonetheless, this attenuation could be enhanced by stimulation with relevant cytokines. In conclusion, these findings demonstrate that the sensory nerve EP4 may regulate angiogenesis through Efnb2-mediated Dll4-associated Notch signaling during HO (see Figs 5 and 6).

2.5. Inhibition of EP4 attenuates the progression of HO

To investigate the involvement of sensory nerve EP4 in the pathogenesis of HO, we administered the EP4 inhibitor CJ-42794, known for its anti-inflammatory and anti-pain effects [24,25]. We injected the inhibitor intraperitoneally in $EP4^{wt}$ mice following tenotomy. Given that sensory nerve infiltration at the tenotomy site becomes detectable one week after trauma [8], we decided to administer injections five times a week for nine consecutive weeks starting one week after the surgical manipulation. We used a dose of 10 mg/kg as the lowest dose across the groups [24], and tested three different doses of inhibitors—low, medium, and high—each at twice the concentration of the previous one to determine the most effective dosage. CT imaging revealed that the high dose of the inhibitor effectively inhibited HO compared to the control and vehicle-treated groups, without significantly affecting normal osteogenesis (Figs. S4A–G). Furthermore, each dose did not cause visible damage to the visceral tissues of the mice (Figs. S4H–L). Based on these findings, we selected the high-dose group as the designated treatment dosage. We then conducted a phenotypic analysis to explore the impact of EP4 inhibition on the pathogenesis of HO. The results of H&E staining, Safranin O-Fast Green staining, and micro-CT revealed a significant reduction in the area of heterotopic ossification (HO) following EP4 inhibition compared to the control and vehicle-treated mice (Fig. 7A–D). Additionally, the expression of H-type vessels, sensory nerves EP4 and *OSX*, were notably diminished (Fig. 7E–G, Figs. S5A–E). Together, these results indicate that EP4 inhibition attenuates HO through the suppression of angiogenesis-associated bone formation.

3. Discussion

Sensory nerves play a pivotal role in gathering signals from within or outside the body, enabling individuals to make appropriate responses to the constantly shifting surroundings [21,26]. HO has been specifically associated with the nervous system, as it occurs following central nervous system (CNS) injury [27]. Prior military statistics provide compelling evidence linking the development of HO to alterations in the peripheral nervous system (PNS) or CNS, indicating that approximately 60 % of combat-related injuries exhibit concomitant HO [28]. This correlation is likely attributed to the prevalence of blast or burn injuries, both of which exert a profound influence on the PNS and CNS. Notably, recent research has unveiled that after soft tissue damage, sensory nerves activated by NGF migrate towards the site of HO [8]. However, the precise mechanism through which sensory nerves then promote ectopic bone formation remains unclear. Previous studies have validated that the sensory nerve EP4/PGE2 signaling pathway not only governs the perception of pain but also influences the process of bone formation. Additionally, sensory nerve EP4 plays a crucial role in shaping the osteogenic commitment of MSCs by modulating sympathetic tones [11]. However, whether the sensory nerve EP4 exerts a crucial role in the pathogenesis of HO remains elusive. In our current study, we found that sensory nerves EP4 expression was remarkably elevated in human HO tissue and post-traumatic HO mice. Additionally, depletion of EP4 in sensory nerves or interruption of EP4 signaling attenuated HO in rodents.

HO is characterized by pathological bone and cartilage formation in soft tissues such as tendons and muscles, rather than in bone tissue itself [1]. However, the process by which MSCs or osteoprogenitor cells reach the Achilles tendon tissue to facilitate ossification during HO pathogenesis remains unknown. Bone formation normally occurs alongside angiogenesis. A unique category of vessels, known as H-type or $CD31^{hi}Emcn^{hi}$ vessels, has recently been identified as facilitators of the interaction between angiogenesis and osteogenesis [29]. Notably, previous studies have shown that H-type vessels establish a positive feedback loop with MSCs at the start of osteoarthritis. These vessels play a critical role in supplying MSCs that contribute to the abnormal bone formation observed during OA progression. In turn, MSCs enhance angiogenesis through the FAK-Grb2-MAPK pathway [13]. This suggests that sensory nerves may regulate the delivery of MSCs or osteoprogenitor cells in subjects with HO by controlling H-type vessels. The interdependence between peripheral nerves and blood vessels is evident, as blood vessels provide nutrients to axons while peripheral nerves regulate vessel caliber [30]. The concept of neurovascular coupling in both normal and abnormal tissue regeneration is gaining increasing attention [31,32]. In this study, we observed a significant increase in sensory nerve EP4 and H-type vessels in both individuals afflicted with HO and in a mouse model of HO. Notably, deleting of EP4 in sensory nerves or the suppressing of EP4 signaling effectively reduced the presence of H-type vessels in the Achilles tendon, thereby impeding the progression of HO. We further assessed the potential side impacts of EP4

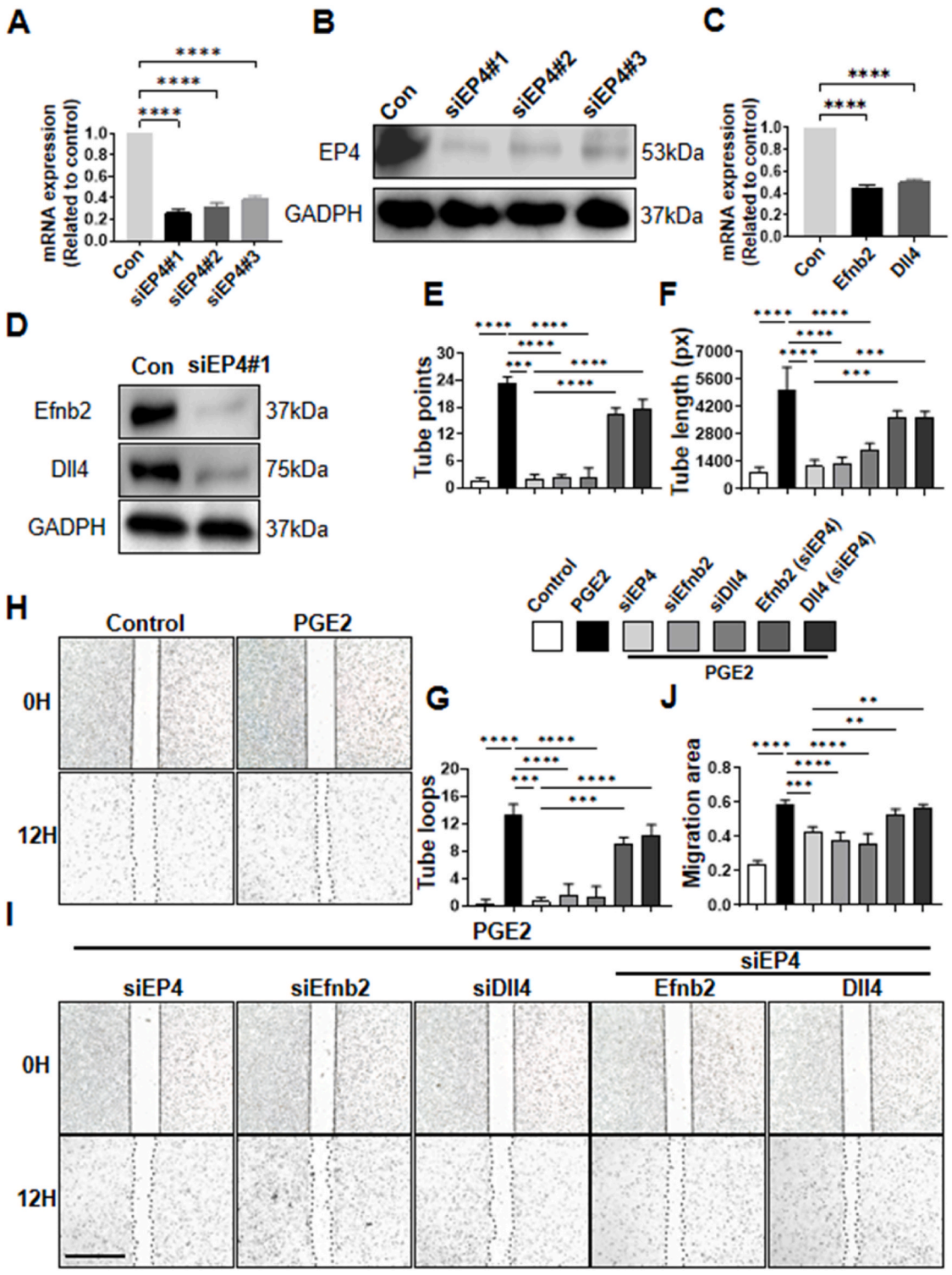

Fig. 6. In vitro study of sensory nerve EP4 promoting vessel formation via the Efnb2/Dll4 axis (A) qRT−PCR examination of mRNA expression of EP4 in SH-SY5Y cells after transfection of siRNA (B) Western blot examination of expression of EP4 in SH-SY5Y cells after transfection of siRNA (C) qRT−PCR examination of mRNA expression of Efnb2 and Dll4 in SH-SY5Y cells after silence of EP4 by transfection of siRNA (D) Western blot examination of expression of Efnb2 and Dll4 after silence of EP4 by transfection of siRNA (E–G) The tube formation assay using supernatants of SH-SY5Y cells treated with different methods. Control: supernatants from SH-SY5Y without stimulation of PGE2; PGE2: supernatants from SH-SY5Y with stimulation of PGE2 for 1h; siEP4: supernatants from SH-SY5Y with stimulation of PGE2 after silence of EP4; siEfnb2: supernatants from SH-SY5Y with stimulation of PGE2 after silence of Efnb2; siDII4: supernatants from SH-SY5Y with stimulation of PGE2 after silence of Dll4; Efnb2: supernatants from SH-SY5Y with stimulation of PGE2 and Efnb2 after silence of EP4; Dll4: supernatants from SH-SY5Y with stimulation of PGE2 and Dll4 after silence of EP4. Scale bar, 200 μm (H, I) Scratch wound assay using supernatants of SH-SY5Y cells under different conditions as mentioned above (J) Quantification of migration area of BMECs under different conditions in scratch assay (ns $p > 0.1$ ***$P < 0.001$ ****$P < 0.0001$ compared to the control group or as denoted by bars).

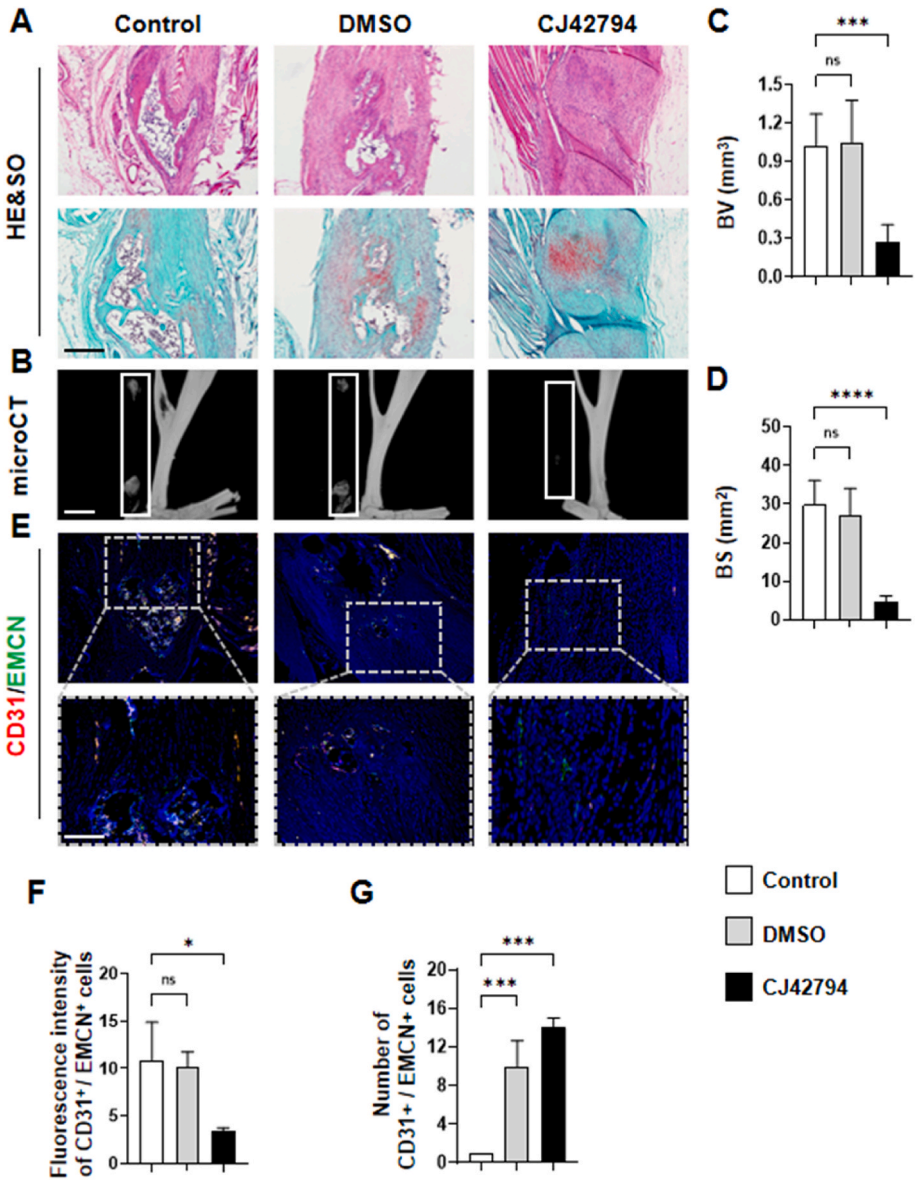

Fig. 7. Blocking EP4 mitigates the advancement of HO (A) H&E staining and Safranin O and Fast Green (SOFG) staining of mice Achilles tendon (sagittal view) after 10 weeks of traumatic induced HO with respectively saline-treated (control group), vehicle-treated (DMSO) and EP4 inhibitor-treated. Proteoglycan (red) and heterotopic bone (green). Scale bar, 100 μm (B) Micro CT images of ectopic bone formation in mice Achilles tendon (sagittal view) of each treatment group (C, D) Quantitative analysis of bone volume (BV) and bone surface (BS). n = 5. Scale bar, 2 mm (E) Immunostaining of H-type vessels (endomucin: green; CD31: red; merge: yellow) in mice Achilles tendon (sagittal view) of each treatment group. Scale bar, bottom 50 μm; top 100 μm (F, G) Quantification of fluorescence intensity and number of $CD31^{+}/EMCN^{+}$ cells related to control. n = 5 (ns $P > 0.1$ *$P < 0.05$ **$P < 0.01$ ***$P < 0.001$ compared to the control group or as denoted by bars).

inhibition on normal bone formation or whether this gives rise to more extensive denervation. The internal milieu of regular bone and the trauma locus differs. In the traumatic stress condition, the sensory nerves were activated in traumatic site [8], which not only perceives pain, but also governs bone formation in situ [10,11,33]. In clinical observation, patients frequently experience pain at the traumatic locus during ectopic bone formation, whilst no pain exists at the normal bone. That implies that aberrant sensory nerve innervation may not necessarily be affiliated with normal bone. Accordingly, the ablation of EP4 in sensory nerve might inhibit local sensory nerve innervation yet exert no effect on normal bone. As the ablation of EP4 in sensory nerve will give rise to pain alleviation at the trauma site, which might lead to the alteration of the stress response of our body to trauma, such as the secretion of nerve growth factor (NGF), and ultimately lead to a reduction in sensory nerves at the trauma site but not in normal bone. Indeed, our findings support this. Our results of micro-CT and CGRP + nerve fiber staining in the distal tibial adjacent to the trauma site reveals that there is no discrepancy in bone formation and sensory nerve expression between the control and HO groups. These findings suggest that sensory nerve EP4 could potentially influence the development of HO by modulating angiogenesis-mediated bone formation.

In this study, we also explored the specific molecular mechanisms through which sensory nerve EP4 influences vessel formation in HO. We conducted RNA-sequencing and bioinformatics analysis were conducted on lesion tissues of the Achilles tendon obtained at 10 weeks post-surgical induction, employing $EP4^{-/-}_{Avil}$ mice, which are sensory nerve-specific EP4 knockout mice for comparison with $EP4^{lox/lox}$ mice. In accordance with the transcriptome analysis, there exist 37 genes associated with the angiogenesis function among the differentially expressed genes, with the top 5 genes being Meox2, Efnb2, Unc5b, Sema6a, and Cdh5. Mesodermal homeobox-2 (Meox2), also known as Growth Arrest-specific homeoboX (GAX), encodes a homeodomain transcription factor

which is expressed in vascular smooth muscle and ECs, whereupon characterization intimates that it is a preeminent regulatory gene governing the angiogenic phenotype [34–36]. Unc-5 Netrin Receptor B (Unc5b) serves as a dependence receptor in ECs, inducing apoptosis in the absence of its ligand Netrin-1, while upon Netrin-1 binding, it impedes apoptosis, thereby subtly regulating developmental angiogenesis [37–39]. Semaphorin 6A (Sema6a) is reported to be a sort of angiogenesis inhibitor, and the silencing of Sema6a partially reversed the inhibition of endothelial cell sprouting [40]. Additionally, Cdh5 has been ascertained to play an irreplaceable and central role in EC biology [41,42], and it is regarded as a significant target for angiogenesis in Glioblastoma multiforme (GBM) and osteoarthritis [12,43,44]. It has been reported that the bidirectional signaling of Efnb2-Ephb4 is believed to control the transition from bone resorption to bone formation, which is important for maintaining bone homeostasis [45]. Additionally, within the tumor microenvironment, Ephb4 and Efbb2 have opposing effects, with elevated EphB4 levels and decreased Efnb2 levels correlating with reduced angiogenesis in tumors and extended patient survival [46]. This suggests that Efnb2 may enhance angiogenesis. The reason for our selection of Efnb2 as the targeted gene in this research relies on that Efnb2 not merely holds a high rank in angiogenesis, but also situates within the top 20 of all differentially expressed genes, as depicted in Fig. 5F. Other genes ranking highly in angiogenesis, as aforementioned, are also exceptionally fine angiogenesis genes responding to EP4 signaling. We will further explore their potential functions in sensory nerve EP4 regulating HO in future researches. In a further exploration through the PPI network, we discovered that the *Efnb2* gene had the strongest association with *Dll4* gene among all notable differentially expressed genes, with Efnb2 exerting a positive regulatory influence on Dll4. Notably, Dll4 is a crucial ligand in the classical Notch-signaling cascade, a pathway known for its significant role in the formation of H-type vessels [14]. Herein, we confirmed a notable upregulation in the levels of Efnb2 and Dll4 expression at the trauma site of the Achilles tendon during HO in $EP4^{lox/lox}$ mice in comparison to $EP4^{-/-}_{Avil}$ mice. Our in vitro findings further manifested that the sensory nerve facilitates vessel formation, while this function was hindered when inhibiting its Efnb2 or Dll4 signaling by means of the relevant interfering RNA. Meanwhile, we discovered that the deletion of EP4 in the sensory nerve inhibits its role in vessel formation; however, Efnb2 or Dll4 stimulation has the ability to reverse this phenomenon. By integrating the in vitro and in vivo assays, we validated that the sensory nerve EP4 promotes ectopic bone formation through modulating Efnb2/Dll4 signaling during HO. It is another exceedingly good research subject concerning how sensory nerve EP4 regulates the Efnb2/Dll4 axis, and we will further explore the related molecular mechanisms in future researches. These findings suggest that the sensory nerve EP4 could potentially modulate H-type vessel formation through Efnb2-mediated Dll4-associated Notch signaling in the context of HO.

Concerning the transection of the sciatic nerve, there are numerous researches investigating the impact of sciatic nerve transection on HO [8,21], nevertheless, whether the sciatic nerve transection affects the angiogenesis-related bone formation has not been explored during the onset of HO. Our findings manifested that transection of the sciatic nerve lead to a notable reduction of H-type vessels and ectopic bone formation in the Achilles. Truly, the sciatic nerve encompasses sensory nerve and motor nerve. The reason for choosing the sensory nerve depends on the fact that previous research has disclosed that the sensory nerve possesses the capacity to modulate bone formation [10,33]. And our findings also disclosed that during the advent of HO, the sensory nerve augmented at the site of HO and the regulation of the sensory nerve function played a crucial role in HO. It is indeed possible that motor nerves exert an influence on HO. We will further conduct relevant studies with respect to the impact of motor nerve on HO in future investigations.

In summary, we observed an increase in sensory nerve EP4 and H-type vessels during the development of HO in both human subjects and mice. Disrupting EP4 specifically in sensory nerves impedes angiogenesis-driven bone formation and the progression of HO. Furthermore, the Efnb2/Dll4 axis has been identified as a downstream element of sensory nerve EP4 modulation of angiogenesis-dependent bone formation. Based on these findings, sensory nerve EP4 holds great promise as a potential approach to attenuate HO.

4. Materials and methods

4.1. Animals use and experimental model

All 3-month-old male C57BL/6J (WT) mice (n = 5) were obtained from the animal center of Southern Medical University, Guangzhou, China. Surgical procedures involving Achilles tendon (AT) surgery were performed on the right ankle of each mouse under the guidance of a surgical loupe. Following surgery, the mice were randomly assigned to plastic cages according to their body weight and the experimental protocol, enabling free movement within the cages.

In certain experiments, surgical denervation was conducted concurrently with heterotopic ossification (HO) induction. A superficial vertical incision was made on the femur to access the target region. Upon opening the skin, a distinct white line corresponding to the fascia between the muscles was identified. A small incision was made along this linea alba, followed by careful dissection until the fascia was elevated and the sciatic nerve trunk was exposed. Subsequently, the sciatic nerve was severed, and the muscle layer, subcutaneous tissue, and skin were sequentially sutured. As a control, sham nerve injuries involved surgical exposure of the sciatic nerve without actual transection [8].

LoxP-flanked EP4 and Advillin-Cre were obtained from Cyagen (Stock No.017986, China). First, mice carrying loxP-flanked EP4 alleles ($EP4^{lox/lox}$) and Advillin-Cre transgenic mice were crossed to obtain Advillin-$CreEP4^{lox/-}$ mice, which were then mated with $EP4^{lox/lox}$ mice to obtain Advillin-$CreEP4^{lox/lox}$ mice ($EP4^{-/-}_{Avil}$). For the sensory nerve-specific EP4 knockout experiment, 3-month-old male $EP4^{lox/lox}$ mice and $EP4^{-/-}_{Avil}$ mice were used to perform Achilles tenotomy to observe post-traumatic HO in each independent experiment (n = 3 per group). PCR analyses of genomic DNA were used to determine the genotypes of the mice using the primers shown in Table 1.

To achieve systemic inhibition of EP4 in C57BL/6J mice, we utilized the EP4 inhibitor CJ-42794 (MedChem Express, China). For administration of CJ-42794, mice were intraperitoneally injected with 100 μl of the compound mixture five days per week at doses of 10, 20, and 30 mg/kg. This treatment regimen commenced one week following Achilles tendon transectional surgery and continued for a duration of nine weeks. For preparation of the injection, 100 μL of a DMSO (Solarbio, China) solution containing CJ-42794 (dissolved in 400 μL of PEG300 (Solarbio, China)) was combined with 50 μL of Tween-80 (Solarbio, China). Sterile saline was then added to adjust the volume to 1 mL.In all cases, amounts of 100 μl normal saline (NS) and 2 % DMSO were used as control and vehicle groups, respectively. The experimental procedures were sanctioned by the Institutional Animal Care and Use Committee of Southern Medical University.

Table 1
The primer sequences used to determine the genotypes of the mice.

Gene name	Sequence
EP4 (Gene bank: 19219)	
forward	TCTGTGAAGCGAGTCCTTAGGCT
reverse	CGCACTCTCTCTCTCCCAAGGAA
Advillin (Gene bank: 11567)	
forward	CCCTGTTCACTGTGAGTAGG
reverse	GCGATCCCTGAACATGTCCATC

4.2. Human specimens

Human samples were obtained from patients undergoing surgery for internal fixation of elbow fractures. The selected patients, aged 20–40 years, were free from osteoporosis and exhibited symptomatic radiographic elbow HO without any concurrent systemic diseases (n = 5). Ectopic bone tissue from the specimens was utilized for the HO group, while adjacent muscle tissue served as the control group. The specimens underwent CT scanning and histological analysis. All personal information was anonymized. Ethical approval for this study was obtained from the medical ethics committee of Nanfang Hospital.

4.3. Cell line and cell transfection

SH-SY5Y cells, a type of neural cell line derived from human neuroblastoma that a number of researchers use to study the function of sensory nerves [47–49], and bone marrow endothelial cells (BMECs) were cultured separately in DMEM-F12 (Gibco, USA) and DMEM (Gibco, USA), supplemented with 100 mg/mL streptomycin sulfate (Life Technologies, USA), 15 % fetal bovine serum (FBS; Procell, China), and 100 U/mL penicillin. The small interfering RNA (siRNA) used for gene knockdown was provided by Tsingke (Beijing, China), with the specific sequences detailed in Table 2. SH-SY5Y cells at 60 % confluence in 6-well plates were transfected with EP4 knockdown siRNAs (siEP4#1, siEP4#2, siEP4#3), Efnb2 knockdown siRNA (siEfnb2), or Dll4 knockdown siRNA (siDll4) using transfection reagents from Tsingke. Total RNA was extracted from the transfected cells after 48 h, and protein was extracted after 72 h. After incubating SH-SY5Y cells in serum-free medium for 1 h, either with or without gene knockdown, the supernatant was collected and promptly stored at −80 °C to obtain the conditioned medium. The certain amount of stimuli [50–52] used to treat the SH-SY5Y cells included PGE2, Efnb2, and Dll4 (MedChem Express, China), all of which were dissolved in cell-grade DMSO (Solarbio, China).

4.4. Migration assay

The wound scratch assay was employed to evaluate the migration of BMECs in response to various conditioned media from SY5Y cells. In this procedure, 5 × 10^5 cells were plated into a 6-well dish and allowed to reach full confluence. Following a 24-h incubation at 37 °C, a sterile p200 pipette tip was used to carefully create a scratch. Cell images were taken at 0 and 12 h post-injury. The ImageJ software was then used to accurately quantify the changes in the width of the scratched regions. The migration rate within the targeted areas was calculated using the formula: Migration area (%) = (A0–An)/A0 × 100, where A0 represents the initial wound area, and An denotes the wound area remaining at the time of measurement.

Table 2
The target sequences used for gene knockdown.

siEP4#1	
sense	GGAGCAGAAAGAGACGACC
antisense	GGUCGUCUCUUUCUGCUCC
siEP4#2	
sense	GUGGUGCGAGUGUUCAUUA
antisense	UAAUGAACACUCGCACCAC
siEP4#3	
sense	CAGGCACUGUGUGACUAUA
antisense	UAUAGUCACACAGUGCCUG
siEfnb2	
sense	GGAAGAAGUUCGACAACAATT
antisense	UUGUUGUCGAACUUCUUCCTT
siDll4	
sense	GUGACAAGAGCUUAGGAGA
antisense	UCUCCUAAGCUCUUGUCAC

4.5. Tube formation assay

BMECs were seeded at a density of 2 × 10^4 cells per well into 96-well plates that had been pre-coated with 60 μL of Matrigel per well (Corning, USA). The plates were then incubated at 37 °C in various conditioned medium. After 4 h of incubation, the cells were imaged and analyzed using an inverted microscope (Olympus) and Image-Pro Plus 6 software. The analysis included measurements of total loops, total branching points, and total tube length.

4.6. Western blot assay

The samples involved in protein detection include human ectopic bone tissue, mouse Achilles tendon tissue and SH-SY5Y cells, using Bone Tissue Protein Extraction Kit (Bestbio, BB-3161, China) and Total Protein Extraction Kit (Bestbio, BB-3101, China). The protein levels were quantified using the PierceTM BCA Protein Assay Kit (Thermo Fisher Scientific, USA). Following protein extraction, supernatants were subjected to sodium dodecyl sulfate-polyacrylamide gel electrophoresis (SDS-PAGE) (Yamei, PG110-114, China), and subsequently transferred onto polyvinylidene fluoride (PVDF) membranes. After blocking with skim milk, primary antibodies were incubated with the membranes overnight at 4 °C. Membranes were then washed three times with TBST (10 min each) and incubated with either goat anti-mouse IgG (1:10,000) or goat anti-rabbit IgG (1:10,000) at room temperature for 60 min. Following another round of washing (three times, 10 min each), protein visualization was performed using the Enhanced Chemiluminescence (ECL Kit; Amersham Biosciences, USA). The antibodies and inhibitors used for Western blotting were as follows: EP4 (Santa Cruz, 1:500, sc-55596, USA), CGRP (Santa Cruz, 1:500, sc-57053, USA), COX2 (Proteintech, 1:500, 12375-1-AP, USA), Efnb2 (Santa Cruz, 1:500, sc-398735, USA), Dll4 (Proteintech, 1:500, 21584-1-AP, USA), goat anti-mouse IgG HRP (Invitrogen, 1:10,000, 31430, USA), and goat anti-rabbit IgG HRP (Invitrogen, 1:10,000, 31460, USA).

4.7. Quantitative real-time polymerase chain reaction analysis

The RNA extraction was performed using TRIzol Reagent (Invitrogen, Carlsbad, CA) in accordance with the manufacturer's protocol, resulting in the isolation of total RNA. Subsequently, 1 mg of the total RNA was utilized for cDNA synthesis with a cDNA Synthesis kit (Fermentas, Burlington, Canada). Following this, qRT−PCR was conducted using FastStart Universal SYBR Premix ExTaqTM II (TaKaRa Biotechnology, Japan). Relative gene expression was quantified using the $2^{-\triangle\triangle CT}$ method. The relative primer sequences were shown in Table 3.

4.8. Histology and immunofluorescence

Human or rodent specimens were collected and fixed in 4 % paraformaldehyde at 4 °C for 24 h. After washing thrice with PBS, samples underwent decalcification in 10 % EDTA (pH 7.4, volume ratio 1:15; Leagene, China) for 21 days at 4 °C. Subsequently, specimens were either embedded in paraffin or OCT (optimal cutting temperature;

Table 3
The primer sequences selected for qRT−PCR.

Gene name	Sequence
EP4 (Gene bank: 5734)	
forward	TACTCATTGCCACCTCCCTGGT
reverse	GACTTCTCGCTCCAAACTTGGC
Efnb2 (Gene bank: 1948)	
forward	GCAAGTTCTGCTGGATCAACCAG
reverse	GCTGTTGCCGTCTGTGCTAGAA
Dll4 (Gene bank: 54567)	
forward	CTGCGAGAAGAAAGTGGACAGG
reverse	ACAGTCGCTGACGTGGAGTTCA

Sakura Finetek, Netherlands) compound. Sagittal sections of the Achilles tendon were obtained at thicknesses of 4 or 40 μm using either paraffin sections or cryosections. Paraffin embedding was exclusively used for human HO tissue. Thin paraffin sections (4 μm) were utilized for all histochemical stains and immunofluorescence analysis of H-type vessels, while thick cryosections (40 μm) were employed for immunofluorescence examination of sensory nerves. For cryosections, samples were individually dehydrated in graded sucrose (20 % and 30 %) overnight at 4 °C before embedding in OCT. Sagittal sections were mounted on adhesive slides (Citotest, China). Histochemical staining included Hematoxylin and eosin (H&E) staining and Safranin O/Fast green staining to assess ectopic bone tissue in the Achilles tendon. After dehydration in ethanol, tissue samples were mounted, and images were acquired using a microscope (Olympus, Japan). Immunofluorescence analysis involved primary antibodies against Endomucin (Santa Cruz, 1:50, sc-65495), CD31 (Abcam, 1:200, ab222783, USA), EP4 (Proteintech, 1:100, 24895-1-AP, USA), CGRP (Santa Cruz, 1:100, sc-57053, USA), Efnb2 (Santa Cruz, 1:100, sc-398735, USA), Dll4 (Proteintech, 1:100, 21584-1-AP, USA) and OSX (Santa Cruz, 1:50, sc-393325, USA) incubated at 4 °C overnight. Secondary antibodies conjugated with fluorescence tags were then incubated at room temperature for 1 h in the dark. Nuclei were stained with 4′,6-diamidino-2-phenylindole mounting solution (DAPI, Servicebio, China) prior to imaging. The entire HO area of the sections was microphotographed for histomorphometric analysis using an Olympus fully automated fluorescence microscope (Olympus BX63, Japan). Quantitative analysis was conducted in a blinded manner using ImageJ software.

4.9. Microcomputed tomography analysis

Following dissection, ankle joints were immersed in a 10 % formaldehyde solution overnight for fixation. Subsequently, the samples were subjected to high-resolution micro-computed tomography (CT) scanning using a SkyScan 1172 apparatus, coupled with CT reconstruction software (NRecon v1.6). Three-dimensional model visualization and additional data analysis were performed utilizing CTAn v1.9 and μCTVol v2.0. The scanning parameters were set at 50 kVp voltage, 200 μA current, and a pixel resolution of 9 μm. The entire ectopic bone area of the specimens was selected as the region of interest, bone volume (BV) and bone surface (BS) was quantified for each experimental group. Epiphysis of distal tibia in mice was selected as the region of interest, trabecular number (Tb.N), trabecular separation (Tb.Sp) and trabecular thickness (Tb.Th) was quantified for each experimental group.

4.10. Sequencing of mRNA and bioinformatics analysis

Total RNA was extracted using the Trizol reagent kit (Invitrogen, Carlsbad, USA) in accordance with the manufacturer's guidelines. The integrity of RNA was evaluated utilizing an Agilent 2100 Bioanalyzer (Agilent Technologies, Palo Alto, USA) and verified through RNase-free agarose gel electrophoresis. Following this, eukaryotic mRNA was enriched employing Oligo(dT) beads. The enriched mRNA was subsequently fragmented into shorter segments using fragmentation buffer and transcribed in reverse into cDNA using the NEBNext Ultra RNA Library Prep Kit for Illumina (NEB#7530, New England Biolabs, Ipswich, USA). The resultant double-stranded cDNA fragments underwent processes including end repair, A-base addition, and ligation with Illumina sequencing adapters. The ligation reaction underwent purification using AMPure XP Beads (1.0×) and underwent amplification via polymerase chain reaction (PCR). The generated cDNA library was subjected to sequencing on the Illumina Novaseq6000 platform by Gene Denovo Biotechnology Co (Guangzhou, China). Differential expression analysis of RNAs was conducted using DESeq2 [53] software for inter-group comparisons, while edgeR [54] was employed for intra-group comparisons. Genes/transcripts exhibiting a false discovery rate (FDR) parameter below 0.05 and an absolute fold change of ≥2 were considered differentially expressed genes/transcripts. Gene Ontology (GO) enrichment analysis was performed to identify significantly enriched GO terms among the differentially expressed genes relative to the genome background. Initially, all differentially expressed genes were aligned with GO terms in the Gene Ontology database (http://www.geneontology.org/), and the number of genes associated with each term was calculated. Significantly enriched GO terms within the differentially expressed genes relative to the genome background were identified using the hypergeometric test. Subsequently, the resulting p-values underwent FDR correction, with a threshold of FDR ≤0.05 considered significant. GO terms meeting this criterion were recognized as significantly enriched.

4.11. Statistics

The data are expressed as mean ± standard deviation (s.d.). To compare two groups, a two-tailed Student's t-test was utilized. For comparisons involving multiple groups, we employed one-way analysis of variance (ANOVA). Initially, we assessed the homogeneity of variance and subsequently examined inter-group differences using post hoc multiple comparisons. Specifically, Dunnett's T3 test was utilized to assess group variations in the presence of heterogeneity. Conversely, the Bonferroni test was applied when no heterogeneity was observed. Statistical significance was set at $P < 0.05$. All data analyses were conducted using SPSS 22.0 analysis software (SPSS, Inc.).

Funding information

This study was supported by National Natural Science Foundation of China (82272250 to ZC and 81830079 to BY), Natural Science Foundation of Guangdong Province, China (2024A1515012533 to ZC), Science and Technology program of Guangzhou (202002030483 to ZC), Outstanding Youths Development Scheme of Southern Medical University (2021YQPY008 to ZC), Guangdong Basic and Applied Basic Research Foundation (2022A1515110904 to HW).

CRediT authorship contribution statement

Z. C. **(Zhuang Cui)**, R.L. **(Rongmin Lin)**, H.W. **(Hangtian Wu)** and T.X. **(Ting Xu)** conceived and designed the study; R.L. **(Rongmin Lin)**, H.L. **(Hancheng Lin)**, J.H. **(Jiahui Hou)**, C.Z. **(Chencheng Zhu)**, J.Z. **(Jieming Zeng)**, Y.T. **(Yihui Tan)**, X.Z. **(Xuyou Zhou)** and Y.M. **(Yuan Ma)** performed the experiments; T.X., R.L., K.W. **(Kuanhai Wei)**, H.L., J.H. and M.Y. **(Mankai Yang)** analysed the data; B.Y. **(Bing Yu)**, R.L., H. W. and Z.C. wrote and revised the manuscript. All authors reviewed and agreed upon the manuscript.

Declaration of competing interest

The authors have declared that no competing interests exist.

Appendix A. Supplementary data

Supplementary data to this article can be found online at https://doi.org/10.1016/j.jot.2024.09.005.

References

[1] Vanden BL, Vanderstraeten G. Heterotopic ossification: a review. J Rehabil Med 2005;37:129–36.
[2] Wang X, Li F, Xie L, Crane J, Zhen G, Mishina Y, et al. Inhibition of overactive tgf-beta attenuates progression of heterotopic ossification in mice. Nat Commun 2018;9:551.
[3] Shehab D, Elgazzar AH, Collier BD. Heterotopic ossification. J Nucl Med 2002;43:346–53.
[4] Prasad N, Ali A, Stanley D. Total elbow arthroplasty for non-rheumatoid patients with a fracture of the distal humerus: a minimum ten-year follow-up. Bone Joint Lett J 2016;98-B:381–6.

[5] Mavrogenis AF, Soucacos PN, Papagelopoulos PJ. Heterotopic ossification revisited. Orthopedics 2011;34:177.
[6] Agarwal S, Loder S, Cholok D, Peterson J, Li J, Fireman D, et al. Local and circulating endothelial cells undergo endothelial to mesenchymal transition (endmt) in response to musculoskeletal injury. Sci Rep 2016;6:32514.
[7] Agarwal S, Loder S, Brownley C, Cholok D, Mangiavini L, Li J, et al. Inhibition of hif1alpha prevents both trauma-induced and genetic heterotopic ossification. Proc Natl Acad Sci U S A 2016;113:E338–47.
[8] Lee S, Hwang C, Marini S, Tower RJ, Qin Q, Negri S, et al. Ngf-trka signaling dictates neural ingrowth and aberrant osteochondral differentiation after soft tissue trauma. Nat Commun 2021;12:4939.
[9] Salisbury E, Rodenberg E, Sonnet C, Hipp J, Gannon FH, Vadakkan TJ, et al. Sensory nerve induced inflammation contributes to heterotopic ossification. J Cell Biochem 2011;112:2748–58.
[10] Chen H, Hu B, Lv X, Zhu S, Zhen G, Wan M, et al. Prostaglandin e2 mediates sensory nerve regulation of bone homeostasis. Nat Commun 2019;10:181.
[11] Hu B, Lv X, Chen H, Xue P, Gao B, Wang X, et al. Sensory nerves regulate mesenchymal stromal cell lineage commitment by tuning sympathetic tones. J Clin Invest 2020;130:3483–98.
[12] Cui Z, Wu H, Xiao Y, Xu T, Jia J, Lin H, et al. Endothelial pdgf-bb/pdgfr-beta signaling promotes osteoarthritis by enhancing angiogenesis-dependent abnormal subchondral bone formation. Bone Res 2022;10:58.
[13] Hu Y, Wu H, Xu T, Wang Y, Qin H, Yao Z, et al. Defactinib attenuates osteoarthritis by inhibiting positive feedback loop between h-type vessels and mscs in subchondral bone. J Orthop Translat 2020;24:12–22.
[14] Ramasamy SK, Kusumbe AP, Wang L, Adams RH. Endothelial notch activity promotes angiogenesis and osteogenesis in bone. Nature 2014;507:376–80.
[15] Russo AF, Hay DL. CGRP physiology, pharmacology, and therapeutic targets: migraine and beyond. Physiol Rev 2023;103(2):1565–644.
[16] Ni S, Ling Z, Wang X, Cao Y, Wu T, Deng R, et al. Sensory innervation in porous endplates by netrin-1 from osteoclasts mediates pge2-induced spinal hypersensitivity in mice. Nat Commun 2019;10:5643.
[17] O'Connor JP, Lysz T. Celecoxib, NSAIDs and the skeleton. Drugs Today 2008;44 (9):693–709.
[18] Blackwell KA, Raisz LG, Pilbeam CC. Prostaglandins in bone: bad cop, good cop? Trends Endocrinol Metabol 2010;21(5):294–301.
[19] Salari P, Abdollahi M. Controversial effects of non-steroidal anti-inflammatory drugs on bone: a review. Inflamm Allergy - Drug Targets 2009;8(3):169–75.
[20] Xue P, Wang S, Lyu X, Wan M, Li X, Ma L, et al. Pge2/ep4 skeleton interoception activity reduces vertebral endplate porosity and spinal pain with low-dose celecoxib. Bone Res 2021;9:36.
[21] Pinho-Ribeiro FA, Verri WJ, Chiu IM. Nociceptor sensory neuron-immune interactions in pain and inflammation. Trends Immunol 2017;38:5–19.
[22] Michel PA, Kronenberg D, Neu G, Stolberg-Stolberg J, Frank A, Pap T, et al. Microsurgical reconstruction affects the outcome in a translational mouse model for achilles tendon healing. J Orthop Translat 2020;24:1–11.
[23] Yu Y, Wang J, Sun Z, Chen Z, Xiong W, Li Y, et al. 0d amplification strategies reshape bone interface niches via biointernalization effects. Adv Funct Mater 2024: 2311975.
[24] Gahbauer S, Deleon C, Braz JM, Craik V, Kang HJ, Wan X, et al. Docking for ep4r antagonists active against inflammatory pain. Nat Commun 2023;14:8067.
[25] Murase A, Okumura T, Sakakibara A, Tonai-Kachi H, Nakao K, Takada J. Effect of prostanoid ep4 receptor antagonist, cj-042,794, in rat models of pain and inflammation. Eur J Pharmacol 2008;580:116–21.
[26] Snyder DJ, Bartoshuk LM. Oral sensory nerve damage: causes and consequences. Rev Endocr Metab Disord 2016;17:149–58.
[27] Baird EO, Kang QK. Prophylaxis of heterotopic ossification - an updated review. J Orthop Surg Res 2009;4:12.
[28] Forsberg JA, Pepek JM, Wagner S, Wilson K, Flint J, Andersen RC, et al. Heterotopic ossification in high-energy wartime extremity injuries: prevalence and risk factors. J Bone Joint Surg Am 2009;91:1084–91.
[29] Kusumbe AP, Ramasamy SK, Adams RH. Coupling of angiogenesis and osteogenesis by a specific vessel subtype in bone. Nature 2014;507:323–8.
[30] Carmeliet P, Tessier-Lavigne M. Common mechanisms of nerve and blood vessel wiring. Nature 2005;436:193–200.
[31] Qin Q, Gomez-Salazar M, Cherief M, Pagani CA, Lee S, Hwang C, et al. Neuron-to-vessel signaling is a required feature of aberrant stem cell commitment after soft tissue trauma. Bone Res 2022;10:43.
[32] Qin Q, Lee S, Patel N, Walden K, Gomez-Salazar M, Levi B, et al. Neurovascular coupling in bone regeneration. Exp Mol Med 2022;54:1844–9.
[33] Mei H, Li Z, Lv Q, Li X, Wu Y, Feng Q, et al. Sema3a secreted by sensory nerve induces bone formation under mechanical loads. Int J Oral Sci 2024;16:5.
[34] Gorski DH, Lepage DF, Patel CV, Copeland NG, Jenkins NA, Walsh K. Molecular cloning of a diverged homeobox gene that is rapidly down-regulated during the g0/g1 transition in vascular smooth muscle cells. Mol Cell Biol 1993;13:3722–33.
[35] Gorski DH, Leal AJ. Inhibition of endothelial cell activation by the homeobox gene gax. J Surg Res 2003;111:91–9.
[36] Grigoriou M, Kastrinaki MC, Modi WS, Theodorakis K, Mankoo B, Pachnis V, et al. Isolation of the human mox2 homeobox gene and localization to chromosome 7p22.1-p21.3. Genomics 1995;26:550–5.
[37] Wang R, Wei Z, Jin H, Wu H, Yu C, Wen W, et al. Autoinhibition of unc5b revealed by the cytoplasmic domain structure of the receptor. Mol Cell 2009;33:692–703.
[38] Castets M, Coissieux MM, Delloye-Bourgeois C, Bernard L, Delcros JG, Bernet A, et al. Inhibition of endothelial cell apoptosis by netrin-1 during angiogenesis. Dev Cell 2009;16:614–20.
[39] Guenebeaud C, Goldschneider D, Castets M, Guix C, Chazot G, Delloye-Bourgeois C, et al. The dependence receptor unc5h2/b triggers apoptosis via pp2a-mediated dephosphorylation of dap kinase. Mol Cell 2010;40:863–76.
[40] Urbich C, Kaluza D, Fromel T, Knau A, Bennewitz K, Boon RA, et al. Microrna-27a/b controls endothelial cell repulsion and angiogenesis by targeting semaphorin 6a. Blood 2012;119:1607–16.
[41] Carmeliet P, Lampugnani MG, Moons L, Breviario F, Compernolle V, Bono F, et al. Targeted deficiency or cytosolic truncation of the ve-cadherin gene in mice impairs vegf-mediated endothelial survival and angiogenesis. Cell 1999;98:147–57.
[42] Bach TL, Barsigian C, Chalupowicz DG, Busler D, Yaen CH, Grant DS, et al. Ve-cadherin mediates endothelial cell capillary tube formation in fibrin and collagen gels. Exp Cell Res 1998;238:324–34.
[43] Corada M, Zanetta L, Orsenigo F, Breviario F, Lampugnani MG, Bernasconi S, et al. A monoclonal antibody to vascular endothelial-cadherin inhibits tumor angiogenesis without side effects on endothelial permeability. Blood 2002;100: 905–11.
[44] Liao F, Li Y, O'Connor W, Zanetta L, Bassi R, Santiago A, et al. Monoclonal antibody to vascular endothelial-cadherin is a potent inhibitor of angiogenesis, tumor growth, and metastasis. Cancer Res 2000;60:6805–10.
[45] Zhao C, Irie N, Takada Y, Shimoda K, Miyamoto T, Nishiwaki T, et al. Bidirectional ephrinb2-ephb4 signaling controls bone homeostasis. Cell Metabol 2006;4:111–21.
[46] Bhatia S, Nguyen D, Darragh LB, Van Court B, Sharma J, Knitz MW, et al. Ephb4 and ephrinb2 act in opposition in the head and neck tumor microenvironment. Nat Commun 2022;13:3535.
[47] Morgan K, Sadofsky LR, Crow C, Morice AH. Human trpm8 and trpa1 pain channels, including a gene variant with increased sensitivity to agonists (trpa1 r797t), exhibit differential regulation by src-tyrosine kinase inhibitor. Biosci Rep 2014;34.
[48] Naznin F, Waise T, Fernyhough P. Antagonism of the muscarinic acetylcholine type 1 receptor enhances mitochondrial membrane potential and expression of respiratory chain components via ampk in human neuroblastoma sh-sy5y cells and primary neurons. Mol Neurobiol 2022;59:6754–70.
[49] Xu K, Pan SY, Song JX, Liu XN, An N, Zheng X. Establishment of a novel therapeutic vector targeting the trigeminal ganglion in rats. Drug Des Dev Ther 2016;10: 585–92.
[50] Lee EO, Shin YJ, Chong YH. Mechanisms involved in prostaglandin e2-mediated neuroprotection against tnf-alpha: possible involvement of multiple signal transduction and beta-catenin/t-cell factor. J Neuroimmunol 2004;155:21–31.
[51] Mueller AC, Piper M, Goodspeed A, Bhuvane S, Williams JS, Bhatia S, et al. Induction of adam10 by radiation therapy drives fibrosis, resistance, and epithelial-to-mesenchyal transition in pancreatic cancer. Cancer Res 2021;81:3255–69.
[52] Lopez-Guerra M, Xargay-Torrent S, Fuentes P, Roldan J, Gonzalez-Farre B, Rosich L, et al. Specific notch1 antibody targets dll4-induced proliferation, migration, and angiogenesis in notch1-mutated cll cells. Oncogene 2020;39: 1185–97.
[53] Love MI, Huber W, Anders S. Moderated estimation of fold change and dispersion for rna-seq data with deseq2. Genome Biol 2014;15:550.
[54] Robinson MD, Mccarthy DJ, Smyth GK. Edger: a bioconductor package for differential expression analysis of digital gene expression data. Bioinformatics 2010;26:139–40.